



Kinetic assessment of dry reforming of methane on Pt + Ni containing composite of fluorite-like structure



L.N. Bobrova^{a,*}, A.S. Bobin^{a,b}, N.V. Mezentseva^a, V.A. Sadykov^{a,b}, J.W. Thybaut^c, G.B. Marin^c

^a Boreskov Institute of Catalysis, 630090 Novosibirsk, Russia

^b Novosibirsk State University, 630090 Novosibirsk, Russia

^c Laboratory for Chemical Technology, Ghent University, Krijgslaan 281 S5, B-9000 Ghent, Belgium

ARTICLE INFO

Article history:

Received 25 June 2015

Received in revised form

15 September 2015

Accepted 26 September 2015

Available online 9 October 2015

Keywords:

Methane

Dry reforming

Fluorite-like complex oxide catalyst

Kinetics

ABSTRACT

Methane dry reforming kinetics over the 1.2% Pt/80% Pr_{0.15}Sm_{0.15}Ce_{0.35}Zr_{0.35}O_x + 10%NiO + 10% YSZ catalyst (Pt + Ni/PrSmCeZrO/YSZ) has been assessed. First-order kinetics in methane was found for the forward reaction rate up to an equimolar methane/carbon dioxide feed ratio. The reaction rate was inhibited by adding methane beyond the stoichiometric value. A relatively constant zero reaction order towards CO₂ can be applied when a CO₂ excess of at least 1.5 over the stoichiometric value is employed. The existence of two different activation regimes is evident in Arrhenius plots with an inflection point at about 750 °C. Kinetic parameters for the net rate of CH₄ conversion over the Pt + Ni/PrSmCeZrO/YSZ composite catalyst were also determined by regression. The novel Pt + Ni/PrSmCeZrO/YSZ catalyst was benchmarked against a complex Pt-promoted fluorite-like doped ceria-zirconia oxide sample of similar atomic fractions of the corresponding elements (Pt/PrSmCeZrO/YSZ) in methane dry reforming. The Pt + Ni/SmPrCeZr/YSZ nanocomposite catalyst is regarded to be the most effective on a per unit mass basis. Higher methane conversions and H₂/CO ratios in the synthesis gas were obtained, while only minor differences were observed in the CO₂ conversions.

© 2015 Elsevier B.V. All rights reserved.

1. Introduction

Nowadays, new technologies and devices are required to create renewable and clean energy feasible alternatives. Syngas, being composed of hydrogen and carbon monoxide, is considered as an alternative to conventional fuels in all its applications. It can be used, like natural gas, as a source of hydrogen for fuel cells, or transformed into other hydrocarbon fuels. The production of synthesis gas via dry reforming, leading to synthesis gas with low hydrogen to carbon monoxide ratio, and the pursuit towards stable catalytic materials have received significant attention from the practical and scientific point of view [1]. One of the principal areas of interest in the study of solid oxide fuel cells (SOFCs) is co-generating syngas internally on the anode and electrical power in a SOFC module by a proper selection of the anode material [2–7]. Heat released in the electrochemical reactions due to internal resistance (ohmic) would be sufficient to sustain highly endothermic

CO₂/CH₄ reforming reaction. However, the development of robust anodes without deactivation by coking during internal reforming of methane will require novel approaches based on the recent advances in nanocomposite materials synthesis and characterization [8–11]. To suppress coking that leads to the deterioration of the anode performance at lower temperature, a promising approach is to promote traditional Ni/YSZ cermets by complex oxides with a high oxygen mobility along with small amounts of precious metals (Pt, Pd, Ru). The catalytic properties are strongly affected by the interactions between composite nanoparticles and support [12–20]. Precious metal atoms incorporated into the surface layer of Ni particles provide sites for activating fuel molecules while decreasing the carbon nucleation probability, whereas the complex oxides of the support will transfer oxygen species to active sites, hence, preventing the deactivation by coking [16–20].

In methane steam reforming, the most efficient promoter for Ni/YSZ-based composite catalyst was proved to be Pr(Sm)-doped ceria-zirconia in combination with Pt [17]. Direct reforming of methane attained sufficient level of conversion in the nanocomposite anode of a planar SOFC [17]. Both steam and dry reforming reactions are known to have similar thermodynamic characteristics and proceed according to a very similar mechanism [21,22].

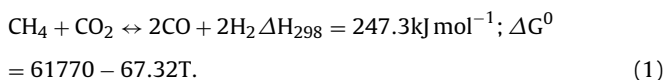
* Corresponding author at: Boreskov Institute of Catalysis 5, Pr. Ak. Lavrentieva, 630090 Novosibirsk, Russia.

E-mail address: lbobrova@catalysis.ru (L.N. Bobrova).

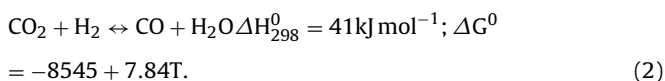
In this paper, studies were conducted to perform a kinetic assessment of methane dry reforming reaction with the 1.2% Pt/80% Pr_{0.15}Sm_{0.15}Ce_{0.35}Zr_{0.35}O_x + 10% NiO + 10% YSZ catalyst. The kinetic parameters for the net rate equation were determined by regression analysis, while mechanistic aspects are considered only briefly here.

2. Theory

The carbon dioxide reforming reaction is highly endothermic and requires higher temperatures being equally favored by a low pressure:



Water is always formed in the reaction. The reverse water gas shift reaction, as a side reaction, is the main water formation route:

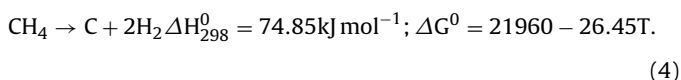


The generalized reaction sequence corresponds to the following overall reaction stoichiometry [1]:



thus, the amount of CO always exceeds that of hydrogen, which means that H₂/CO ratios are below unity. However, upon carbon formation in the methane dry reforming, the H₂/CO ratio is enhanced.

Generally, the coking effect is intimately related to the complex reaction mechanism [23]. The key reaction for carbon deposition leading to increased H₂ production and constant amounts of solid carbon, even at a very high temperature, is methane cracking [24]:



At CO₂/CH₄ > 1, an endothermic reaction of methane decomposition (4) has only a minor effect on carbon deposition, as CH₄ is the limiting reactant. In the temperature range of 557–700 °C and under conditions of stoichiometric CO₂ reforming, carbon deposition may occur via CO disproportionation, i.e., the Boudouard reaction:



while above 820 °C the reverse water–gas shift (2) and the Boudouard Reaction (5) become thermodynamically forbidden. Thereby, carbon deposition is thermodynamically possible for a CO₂–CH₄ reforming feed ratio of 1:1 at temperature up to 870 °C at 1 atm. At a given pressure, the temperature limit increases as the CO₂/CH₄ feed ratio decreases [25]. Topor et al. [26] suggested the use of carbon dioxide excess in the dry reforming reaction. Thus, stable dry methane operation at 650 °C in SOFC using an yttria-doped ceria interlayer between the YSZ electrolyte and the Ni/YSZ cermet anode [27] was found. Using a fuel mixture of 30% methane and 70% carbon dioxide, little carbon fouling and optimum performance of a micro-tubular zirconia cell with lanthanum strontium manganite cathode and nickel/zirconia/ceria anode was obtained, compared to SOFC operating on pure methane [28]. Nevertheless,

in order to maintain a high selectivity towards syngas, CO₂/CH₄ ratios as low as 1:1 are preferred in internal reforming. However, the proper catalyst can kinetically impede carbon formation even at conditions under which the carbon is thermodynamically favorable.

In this study, a 1.2%Pt/80%Pr_{0.15}Sm_{0.15}Ce_{0.35}Zr_{0.35}O_x + 10% NiO + 10% YSZ nanocomposite catalyst (further referred to as Pt + Ni/PrSmCeZrO/YSZ) was tested at 650–850 °C and 1 atm total pressure. Diluted by an inert gas (N₂), methane and CO₂ concentrations were changed over a wide range. Relatively high total flow rates (≥177 ml/min), dilution of the catalytic pellets by quartz within the bed and low conversions of CH₄ and CO₂ ensured that the experimental kinetic data were not obscured by mass transfer limitations and the perfectly mixed conditions allowed for a continuous stirred tank reactor model. Pore resistance effect was estimated by using Wagner–Weisz–Wheeler modulus $M_W = L^2(-R_{\text{CH}_4})_{\text{obs}}/C_{\text{CH}_4}D_e$. The catalyst particle is in the diffusion free regime, if $M_W < 0.15$ [29]. Substituting the appropriate values of molecular diffusivity of CH₄ in the mixture ($D_M = 2.88 \times 10^{-5} \text{ m}^2/\text{s}$) and Knudsen diffusivity computed from Eq. (6) into the Bosanquet relationship (7) we obtained intraparticle effective diffusion coefficient ($D_e = 2.78 \times 10^{-5} \text{ m}^2/\text{s}$) for methane species [30]:

$$D_K = 97r_e \sqrt{\frac{T}{M}} \quad (6)$$

$$D_e = \frac{D_M D_K}{D_M + D_K} \quad (7)$$

according to Eq. (6), the Knudsen diffusivity was calculated from the values of mean pore radius, r_e , absolute temperature, T (in Kelvins), and molecular weight of methane, M .

Given the measured rate, $(-R_{\text{CH}_4})_{\text{obs}}$, characteristic length scale for spherical particles of radius R_{pat} (0.00025 m), $L = R_{\text{pat}}/3$, and the calculated effective diffusion coefficient, D_e , Wagner–Weisz–Wheeler modulus was established to be about 0.03 at 750 °C. Therefore, the reactor was operated in a reaction-limited regime. The diffusion limitation was negligible compared with the reaction rate of methane conversion.

The expansion factor, i.e. the change in the system volume between no conversion and complete conversion amounts to about 0.14 for the 7 vol% CH₄: 7 vol% CO₂ in N₂ reactant feed gas at 30 ms residence time (at STP), which is sufficiently low.

The catalyst activity was assessed through the fractional conversion of reactants x_i defined as the ratio of the number of moles reactant reacted to the number of moles reactant fed. In the constant volume system, this is defined as:

$$x_i = 1 - \frac{C_i}{C_{i0}}, \quad (8)$$

where C_i is the final concentration of i -reactant, C_{i0} is the initial concentration of i -reactant after the reaction takes place.

The product yields were defined as:

$$Y_{\text{H}_2} = \frac{x_{\text{H}_2, \text{out}}}{2 \times x_{\text{CH}_4, \text{in}}} \text{ and } Y_{\text{CO}} = \frac{x_{\text{CO, out}}}{x_{\text{CH}_4, \text{out}} + x_{\text{CO}_2, \text{out}} + x_{\text{CO, out}}}. \quad (9)$$

The molar H₂:CO ratio was obtained from the product gas composition:

$$\text{H}_2 : \text{CO ratio} = \frac{\text{mole of H}_2 \text{ produced}}{\text{mole of CO produced}}. \quad (10)$$

To obtain rigorous values of the forward kinetic rates, the net (overall) rates were corrected for the approach to thermodynamic equilibrium [31,32]:

$$r_f = \frac{r_{\text{exp}}}{(1 - \eta)}, \quad (11)$$

Table 1
Thermodynamic data for CH₄ dry reforming.

	G _{CO} (kJ/mol)	G _{CO₂} (kJ/mol)	G _{CH₄} (kJ/mol)	ΔG _{CORM} (kJ/mol)	K _{eq,CORM} (atm ²)
650	−193.5	−375.7	11.3	−22.5	18.7
700	−197.9	−375.8	16.9	−36.8	94.9
750	−202.3	−375.9	22.5	−51.2	413
800	−206.7	−376	28.3	−65.7	1577.3
850	−211.1	−376.1	34.1	980.2	5377.9

where r_{exp} is the net reaction rate based on unit catalyst surface, e.g. for methane.

$$r_{\text{CH}_4} \left[\frac{\text{mol}}{\text{m}^2 \text{s}} \right] = \frac{x_{\text{CH}_4} \times F_{\text{CH}_4} \left[\frac{\text{mol}}{\text{s}} \right]}{W [\text{kg}] \times S_{\text{sp}} \left[\frac{\text{m}^2}{\text{kg}} \right]} \quad (12)$$

here, x_{CH_4} is fractional conversion of methane, W is a catalyst weight, F_{CH_4} is molar flow of methane, S_{sp} is a specific surface of the catalyst. The approach to equilibrium (η).

$$\eta = \frac{p_{\text{CO}}^2 \times p_{\text{H}_2}^2}{p_{\text{CH}_4} \times p_{\text{CO}_2}} \times \frac{1}{K_{\text{eq,CORM}}} \quad (13)$$

is determined by using thermodynamic data for the reforming Reaction (1). In Eq. (10), p_i represents the partial pressure of species i (in atm), $K_{\text{eq,CORM}}$ are equilibrium coefficients of the CO₂/CH₄ reforming reaction at a given temperature T (Table 1).

$$K_{\text{eq,CORM}} [\text{atm}^2] = \exp \left(-\frac{\Delta G_{\text{CORM}}}{RT} \right) \quad (14)$$

with as Gibbs energy values:

$$\Delta G_{\text{CORM}} = 2G_{\text{CO}} - G_{\text{CO}_2} - G_{\text{CH}_4}$$

$$G_{\text{CO}} = -109.25 - 0.0936 \times T + 2.571 \times 10^{-6} \times T^2$$

$$G_{\text{CO}_2} = -393.9 - 0.002 \times T$$

$$G_{\text{CH}_4} = -76.95 + 0.0807 \times T + 1.617 \times 10^{-5} \times T^2.$$

To analyze the different kinetic schemes derived from the experimental analysis and, hence, elucidate the most appropriate structure for the kinetic equation for the overall rate of CH₄ reforming, a regression analysis has been performed using a data set consisting of 36 measurements. The Athena Visual Studio Software Package (Stewart and Associates Engineering Software, Inc.) was used for this purpose. Via least squares minimization of the squared residuals (SSRs), i.e., the difference between the model simulated and the experimental data, the optimum parameters were determined. Together with the statistical performance of the regression, expressed by the F value for the global significance of the regression and the t values for the individual confidence of the model parameters, the physical meaning of the obtained parameter values was used for the assessment of the adequacy of the various proposed kinetic schemes.

3. Experimental

3.1. Catalyst preparation

Mixed oxide (Pr_{0.15}Sm_{0.15}Ce_{0.35}Zr_{0.35}O_x) as well as yttria-stabilized zirconia (YSZ) were prepared via the organic polymerized complex method, which is a modified version of the polymeric precursor method suggested by Pechini [33]. The method allows preparing homogeneous complex oxides with perovskite and fluorite structure having well controlled properties and a high surface area [34,35]. For the preparation of yttria-stabilized zirconium and

complex oxides, aqueous solutions of starting salts, i.e., nitrates of Y, Sm, Ce and Pr, oxychloride of zirconium, citric acid (CA), ethylene glycol (EG), and ethylene diamine (ED) were employed. The ethylene glycol and citric acid were used as complex formation reagents, ethylene diamine was chosen as additional complex builder as it enhances uniformity. The molar ratio of precursors CA:EG:ED:metal = 3.75:11.25:3.75:1 were used in the preparation of the sol solution. Citric acid has been firstly dissolved in ethylene glycol at a ratio of CA:EG = 1:3 at 60 °C. Aqueous nitrates of metals – Y(NO₃)₃· n H₂O, Ce(NO₃)₃· n H₂O, Pr(NO₃)₃· n H₂O, Sm(NO₃)₃· n H₂O – were dissolved in small amounts of distilled water adding ZrOCl₂ solution thereafter. Ethylene diamine (ED) has then been added drop-by-drop at room temperature (highly exothermic reaction) into the solution obtained after mixing metal nitrates solution and CA/EG mixture. After 2 h, the mixture has been heated above 100 °C to evaporate any trace of water. A very dark and viscous product has been obtained after 4–5 days of polymerization. This petrol-like mass has been further calcined in an air flow furnace at 600 °C for 2 h. The 1.2% Pt/80% Pr_{0.15}Sm_{0.15}Ce_{0.35}Zr_{0.35}O_x + 10% NiO + 10% YSZ nanocomposite catalyst was prepared using two stage. Viscous polymer precursor Pr_{0.15}Sm_{0.15}Ce_{0.35}Zr_{0.35}O_x oxide was prepared on the first stage. On the second stage, an aqueous solution of Ni(NO₃)₂· n H₂O and powder of YSZ were added to polymer precursor of Pr_{0.15}Sm_{0.15}Ce_{0.35}Zr_{0.35}O_x oxide by vigorous stirring with subsequent evaporation and calcination in air at 700 °C for 2 h. Platinum (1.2 wt.% in the nanocomposite catalyst and 1.4 wt.% in the oxide catalyst) was deposited on the support through incipient wetness impregnation with H₂PtCl₆ solution having a concentration of 9.4 mg/ml, followed by drying and calcination for 1 h at 900 °C. The specific surface area was determined by using Ar thermodesorption data obtained on a SORBI-M instrument by the BET (Brunauer, Emmett, Teller) method.

3.2. Catalyst testing

Catalytic activity in the carbon dioxide dry reforming of methane at short residence times (2–30 ms at STP) was studied in a computer-controlled flow installation using 3.5–10.5% CH₄ + 3.5 ÷ 17.6% CO₂ in N₂ feeds for the samples (15.3 and 68 mg) pretreated in flowing dry oxygen at temperatures up to 700 °C for 1 h before the reforming reaction. Next, the reaction mixture was fed until the quasi-stationary concentrations of the products were attained (typically, in 1–3 h), while catalytic measurements were performed. The catalytic samples were placed into a quartz reactor (a tube of 4 mm i.d.) mounted inside a furnace. A thermocouple has been placed into the annular space between the reactor and the furnace. This thermocouple was mounted on the tubular reactor in close contact with the quartz reactor to minimize the temperature difference between the catalyst bed and the thermocouple. In order to improve the isothermicity of the bed, catalyst samples were diluted half and half with silica carbide sand (both in particle size fraction of 0.5–0.25 mm (32–60 mesh)). Reactant and product concentrations were measured on-line with a Test-201 (Bonair, Russia) gas analyzer equipped with IR absorbance, electrochemical and polarographic sensors.

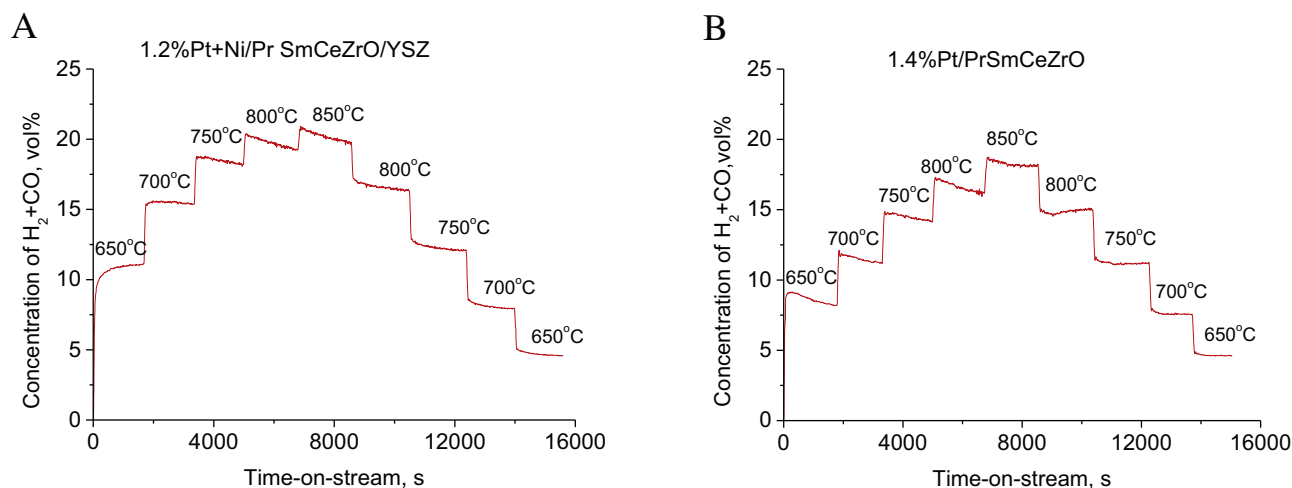


Fig. 1. A check on stability of the compared oxidized catalysts to syngas formation under reaction conditions: a feed mixture—7% CH₄ + 7% CO₂, balance N₂, W/F = 0.025 g s/ml.

4. Results and discussion

4.1. Catalyst features and reaction mechanism

Detailed characteristics of structural and microstructural features of the nanocomposite and oxide catalysts, their surface properties, reactivity and catalytic activity in both steam and dry reforming reactions are given in detail in previous publications [18,35–44] of the authors. Strong interaction between Pt and the nanocrystalline PrSmCeZrO support, i.e., decoration of Pt clusters by support oxidic species, is the most important property which directly influences catalysis. In the as-prepared samples Pt is mainly stabilized as cations incorporated into the surface layers of oxides. There is some sort of interactions between Pt and Ni in the Pt + Ni/PrSmCeZr/YSZ composite catalysts, which is responsible for variations in the dissociative adsorption capacity of methane and carbon dioxide. The pronounced cations redistribution between phases in as-prepared Pt + Ni/PrSmCeZr/YSZ samples results in decoration of NiO nanoparticles by LnZrO fragments with incorporated Pt cations, while mixed oxidic NiPtO clusters are stabilized within the surface of SmPrCeZrO nanodomains. Under reaction conditions, these clusters are transformed into Pt – Ni alloy nanoparticles strongly interacting with support and decorated by support oxidic species. Detailed studies of reaction mechanism of CH₄ dry reforming in stoichiometric feeds on these types of catalysts by kinetic transients, SSITKA, FTIRS and pulse microcalorimetry [39–41] revealed that at steady state conditions reaction mechanism can be satisfactorily described using step-wise redox scheme with independent stages of CH₄ and CO₂ transformation on metal and oxide sites, respectively. These stages are conjugated by fast diffusion of oxygen species from the oxide support sites to the developed metal-support interface. While Pt does not take part in CO₂ activation, Ni atoms are apparently involved in this process, enhancing the ability of the catalyst to be oxidized by CO₂. Isotopic labeling studies have shown that the rate of the catalyst reoxidation by CO₂ as an oxygen supplier greatly exceeds that of its reduction rate by methane. Rapid oxygen redistribution between adsorption sites located on metal and oxide surface occurs during catalysis. It was shown for oxidized Pt-supported catalyst in the unsteady-state conditions, that being strongly adsorbed on basic supports carbon dioxide can be activated through formation of the short-lived surface carbonate species stabilized in vicinity of Pt^{2+/4+} cations. The question whether the carbonate phase participates in the catalytic cycle by providing oxygen which reacts with the carbon issued from methane activated on the metal sites is still open.

4.2. Comparison of the Pt + Ni/PrSmCeZr/YSZ nanocomposite and Pt/PrSmCeZrO oxide catalysts

Preliminary experiments were conducted to check the difference in catalytic performance between the tested Pt + Ni/PrSmCeZrO/YSZ nanocomposite catalyst and the oxide catalyst promoted by Pt. In the previous papers [42–44], the effect of pretreatment, Pt content on the catalytic properties as well as kinetic and mechanistic features of the Pt supported on CeO₂–ZrO₂ oxide composition were already reported.

The catalytic performance of the 1.4% Pt/PrSmCeZrO sample and the studied 1.2% Pt + Ni/PrSmCeZrO/YSZ nanocomposite catalyst are illustrated in Figs. 1–3. The experiments were carried out between 650 °C and 850 °C at atmospheric pressure, under a fixed bed continuous flow. Real time data from the runs in which the temperature was increased up to 850 °C and subsequently decreased again in steps of 50 °C every 30 min to the minimum attainable temperature of 650 °C, are shown in Fig. 1. It can be seen that the activity decreases markedly with run time at any temperature. The temperature effect on catalytic activity of the catalyst based on fluorite-like oxides supports depends on whether the catalyst is fresh or has been previously exposed to the reaction mixture. A progressive

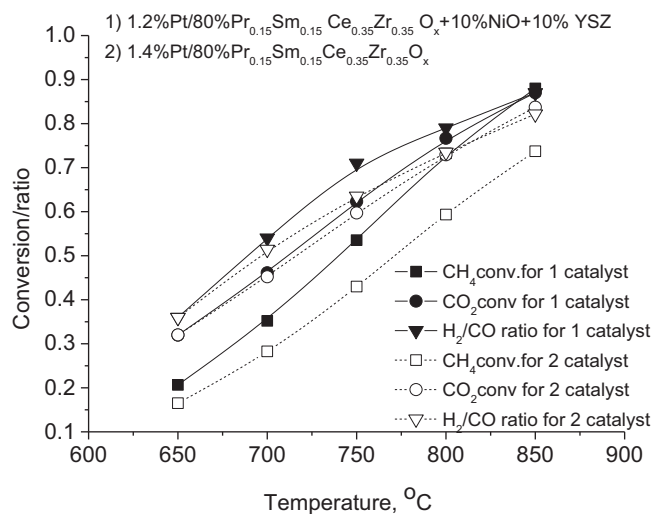


Fig. 2. Effect of the temperature on the CH₄ and CO₂ conversions, the H₂/CO ratio for the compared catalysts: (1) Pt + Ni/PrSmCeZrO/YSZ (density of 1.45 g/cm³); (2) Pt/PrSmCeZrO (density of 1.94 g/cm³).

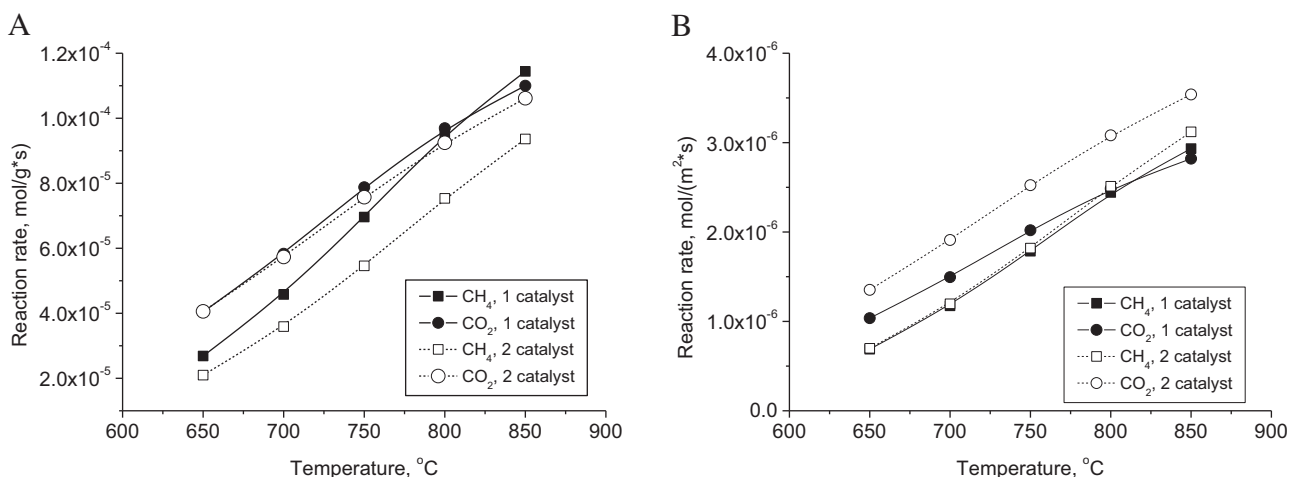


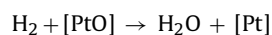
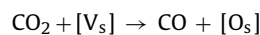
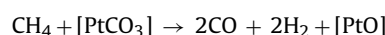
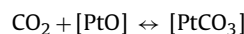
Fig. 3. The CH_4 and CO_2 reaction rates per mass (A) and surface (B) units versus the reaction temperature for a feed mixture – 7% CH_4 +7% CO_2 , balance N_2 , $W/F=0.025$ g s/ml: (1) Pt + Ni/PrSmCeZrO/YSZ ($S_{\text{sp}} = 39$ m 2 /g); (2) Pt/PrSmCeZrO ($S_{\text{sp}} = 30$ m 2 /g).

reduction of the fully oxidized surface occurring during reaction decreases the CH_4 reforming conversion with time-on-stream. While using freshly oxidized catalysts, syngas content in the product is higher, likely due to stored oxygen. Besides, highly disordered structure of the freshly formed clusters of Ni – Pt alloy provides a high efficiency in methane activation, and their ordering due to oxidation under reaction conditions is accompanied by the decrease in catalytic activity. Thereby, an activity enhancement observed during first 2000 s (Fig. 1A) might be associated with reduction and these clusters formation, while the activity further decreases indicating that the ordering surface structure is increased. Such thermal cycling has resulted in stabilization of catalytic activity, thus all kinetic parameters were estimated based on quasi steady-state conditions. It is seen from the data in Fig. 1 that the Ni- Y_2O_3 -stabilized zirconia containing nanocomposite catalyst has a higher syngas production compared to the Pt/PrSmCeZrO oxide catalyst.

The catalytic activities of the samples were evaluated in terms of conversion and net reaction rates of disappearance of CH_4 and CO_2 (Figs. 2 and 3). The runs were conducted at the same catalyst load (39 mg) and equal flow rate (1.57 ml/s). The balanced nitrogen rate was maintained to keep 7% CH_4 + 7% CO_2 in N_2 feeds. Fig. 2 shows the temperature effect on the CH_4 and CO_2 conversions and on the ratio H_2/CO in syngas. The Pt + Ni/PrSmCeZrO/YSZ nanocomposite catalyst (1st catalyst) exhibits considerably higher conversions of methane for all the temperatures as compared to the Pt/PrSmCeZrO oxide catalyst (2nd catalyst). The greater H_2/CO ratio of synthesis gas is also detected in case of the composite with doped NiO and YSZ, while only a small difference is observed in the CO_2 conversions on the two catalysts.

In the comparative experiments, the Ni- Y_2O_3 -stabilized zirconia containing nanocomposite catalyst is more effective on a per unit mass basis than the oxide catalyst (Fig. 3). The rate of the CH_4 conversion over the Pt + Ni/PrSmCeZrO/YSZ sample is more temperature-sensitive than that over the same quantity of the Pt/PrSmCeZrO sample (Fig. 3A). Note that the studied nanocomposite catalyst has somewhat greater specific surface area (39 m 2 /g) than that of oxide catalyst (30 m 2 /g). The trends for reaction rates per unit surface reveal that both the catalysts show comparable activity in the CH_4 disappearance, while higher activity in CO_2 consumption observed for unit surface of the Pt/PrSmCeZrO catalyst over entire temperature range (Fig. 3B) suspected to be originated from the high rate of CO_2 dissociation assisted also by H species generated in CH_4 decomposition and resulted in the water formation route (2).

It is well known, that the catalytic dry reforming reaction benefits from highly dispersed active metal particles (where CH_4 molecules are activated). Both carbon and hydrogen derived from methane react with the surface oxygen species that are at the metal active site/oxide support interface. It is generally agreed that the availability of the mobile oxygen species on the catalyst surface is one of the most important factors affecting the activity and selectivity in the CH_4 dry reforming reaction. This also improves tolerance to coke [45]. In the kinetic scheme (15) proposed for the Pt/PrSmCeZrO oxide catalyst, methane transformation occurs on the active cationic Pt-centers ([PtO] and [PtCO $_3$]), whereas carbon dioxide interacts with [PtO] and oxygen vacancies [V_s] of the support. The main reaction routes (1) and (2) go through the following steps [44]:



The structural studies of the nanocomposites comprised of NiO and YSZ and supported Pt group metals revealed pronounced interaction between constituting phases [17]. Lower rates per surface area for CO_2 conversion observed with the studied Pt + Ni/PrSmCeZrO/YSZ catalyst appeared to be mainly due to suppressing the side reverse water gas shift reaction route. The rate of the CO_2 dissociation reaction depends on the quantity and mobility of oxygen (adsorbed oxygen species, hydroxyl species, or carbonate species) present in the surface. The metal oxidic active species are decorated with fluorite-like oxide fragments, thus weakening bonds between hydrogen and the metal cationic sites. Under reaction conditions, the NiO precursors probably more readily reduced to the metallic Ni segregated particles. This also caused a decrease in oxygen mobility of the fluorite-structured catalytic surface and has inhibitory effect on accessibility of the metal oxidic active species with chemisorbed hydrogen by oxygen-containing species (hydroxyls, hydroxocarbonates, etc.).

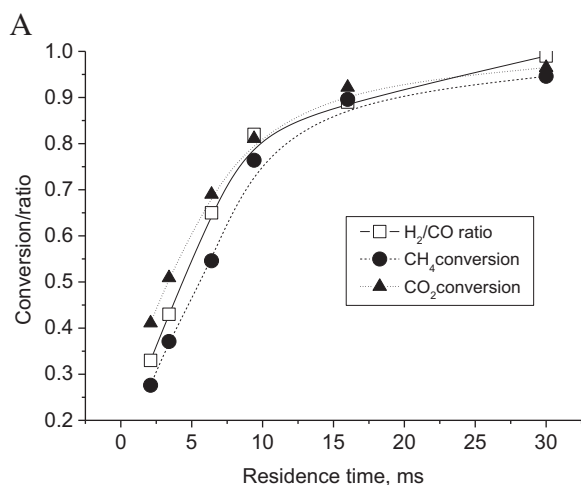


Fig. 4. Effect of the residence time on conversion and H_2/CO ratio (A) and yield of the products (H_2 and CO) at $850^\circ C$: a catalyst – $Pt + Ni/PrSmCeZrO/YSZ$; a feed mixture – $7\%CH_4 + 7\%CO_2$, balance N_2 .

Therefore, the catalytic screening, done at the equal reaction conditions, revealed that the most efficient nanocomposite catalyst with Pt -supported nanoparticles was that comprised of NiO and YSZ . It exhibited the highest activity to CH_4 conversion and syngas selectivity with higher H_2/CO ratio.

4.3. Analysis of kinetic effects over the $Pt + Ni/PrSmCeZrO/YSZ$ catalyst

4.3.1. Effect of residence time

At a given reaction temperature and feed composition, the residence time was varied by changing gas space velocity to achieve different levels of conversion and selectivity. All the study cases (2.1; 3.4; 6.4; 9.4; 16; 30 ms residence times) available for our study have been represented in Fig. 4 to evaluate an effect of the residence time on activity and selectivity of the $Pt + Ni/PrSmCeZrO/YSZ$ catalyst. Evidently, the high residence time is favored for the production of syngas: increasing the residence time increases the reactant conversion, yields of hydrogen and CO , and the H_2/CO molar ratio in syngas. Over the entire range of residence times, the higher H_2/CO molar ratio was observed to be 0.99, and it can be achieved at the residence time of 30 ms. The straight lines within the range of the residence times in Fig. 4B depict the calculated yields at equilibrium for the main products, H_2 and CO , for the given feed stream at the temperature of $850^\circ C$. The graphs plotted in Fig. 4B shows that a residence time of 30 ms was sufficient to achieve equilibrium. Under the prescribed conditions, the experimentally determined hydrogen and carbon oxide yields agree quite closely with these equilibrium values, of 0.84 and 0.95, respectively. In fact, highest conversions, of both CH_4 (0.946) and CO (0.965) were obtained. Conversely, at residence times below 30 ms, the reactor was operated at conditions far from methane dry reforming equilibrium. According to Fig. 4A, decreasing the catalyst residence time (increasing reactor gas space velocity) also presents a negative effect on the selectivity (in terms of yields of hydrogen and CO , and the H_2/CO molar ratio) towards both hydrogen and carbon oxide. However, the main influence was on hydrogen formation and relatively small effect on carbon oxide. Thus, at the residence time of 16 ms, the experimental yields were detected to be lower than equilibrium values by about 11% for hydrogen and by 5% for carbon oxide. This behavior indicates that secondary reactions would likely to occur. Apparently, increasing the residence time facilitates onset of the consecutive reforming reactions, e.g. with active participation of water derived intermediates.

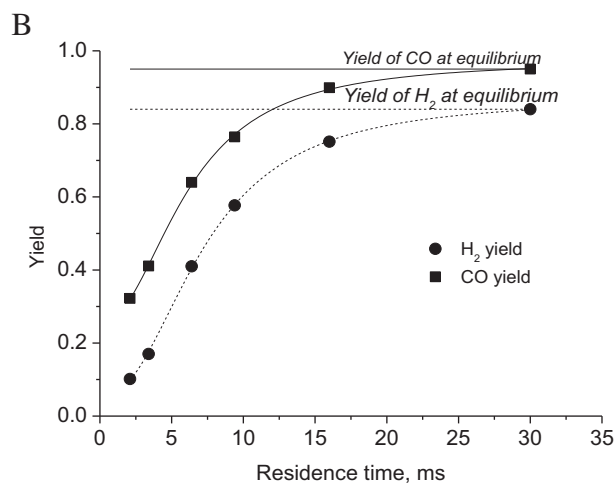


Fig. 5 represents the experimental data at the 30 ms residence time and the corresponding equilibrium-derived data with respect to the effect of reaction temperature. It can be seen that concentrations of CO , H_2 , CH_4 and CO_2 in product gas, approaching those defined by thermodynamic equilibrium at the reaction temperatures $\geq 750^\circ C$.

4.3.2. Effects of variation of the CO_2 and CH_4 feeding concentrations

The effect of CO_2 and CH_4 concentration on the ratio of the components in the product gas at the temperatures of 650 and $850^\circ C$ was investigated by their variation between 3.5 and 17.5 vol%, while keeping the other one constant at about 7 vol% (nitrogen-balance). The results are shown in Figs. 6 and 7.

As shown in Fig. 6A, the H_2/CO ratio in the product gas becomes higher when concentration of CH_4 (the source of hydrogen atoms) increases in the feed. For the specified temperatures, they seem to change with excess of CH_4 at the similar rate. Conversely, the effect of increasing CO_2/CH_4 ratio from 0.5 to 2.5 in the feed (Fig. 6B) is negative for selectivity of the reforming reaction to synthesis gas: the H_2/CO ratios just slightly decrease with excess of CO_2 in the feed. Whenever the temperature is higher, the H_2/CO ratio declines

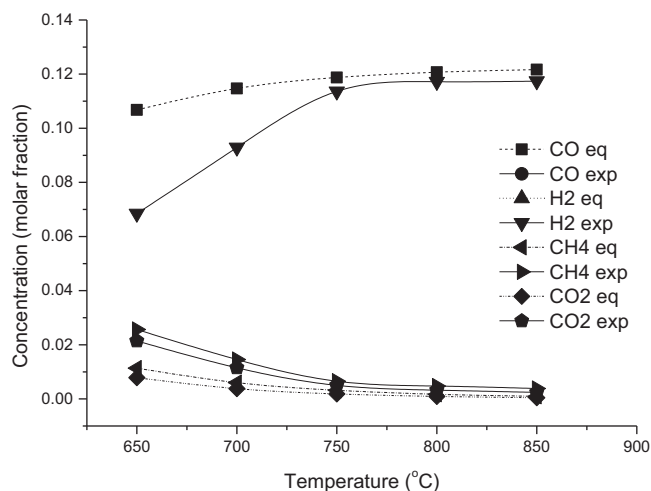


Fig. 5. Concentration of the components in the product gas according experimental observation and thermodynamic equilibria: a catalyst – $Pt + Ni/PrSmCeZrO/YSZ$; a feed mixture – $7\%CH_4 + 7\%CO_2$, balance N_2 ; a residence time – 30 ms.

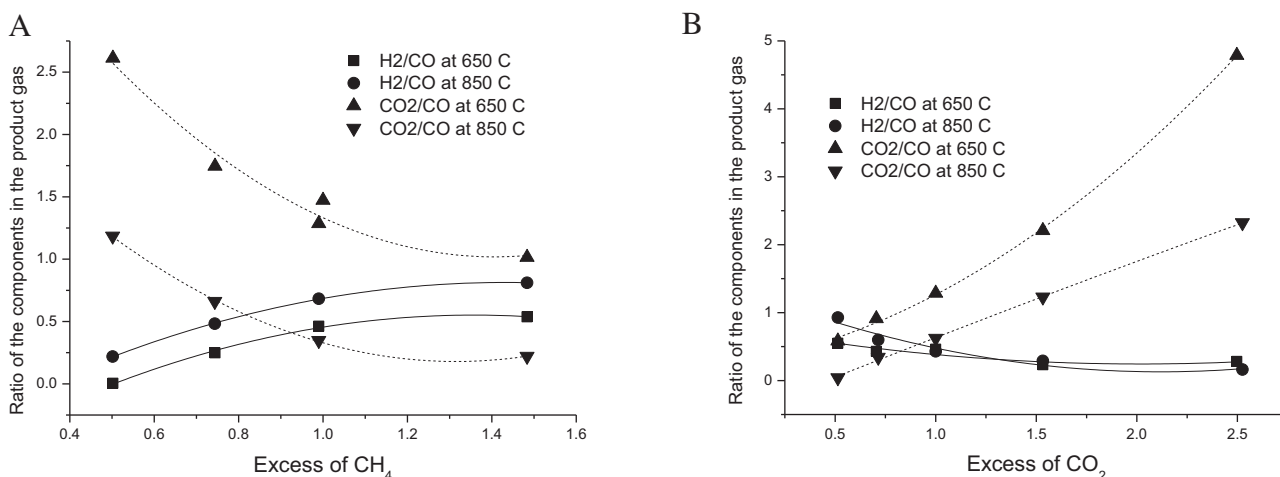


Fig. 6. Molar ratios of H₂/CO and CO₂/CO in the product gas depending on excess of CH₄ (A) and CO₂ (B) over stoichiometric values in the feed: a catalyst – Pt+Ni/PrSmCeZrO/YSZ; a feed mixture – 7% CH₄ + 7% CO₂, balance N₂; W/F=0.0052 g s/ml (3.6 ms residence time).

more intensively. At the temperature of 850 °C, the ratio H₂/CO at CO₂/CH₄ ≥ 1.5 becomes even lower when compared to the corresponding experimental results for 650 °C. The decline in the H₂/CO ratio in syngas is presumably attributed to the side reverse water gas shift reaction (Reaction (2)) in which H₂ produced reacts with CO₂ to form water and CO. On the other hand for CO₂-rich feeds, active site blocking upon accumulation of CO₂ dissociation products may have a far more profound negative effect on selectivity, inhibiting syngas formation. As discussed earlier in this paper, partial oxidation of Ni clusters occurring under the reaction conditions was found to hamper their ability to activate CH₄, thus decreasing the rate of syngas production [40–43].

As shown in Fig. 7A the forward reaction rate for CO₂ is found to be higher than that calculated for CH₄ at the same temperature. The effect of CH₄ excess on the rates of disappearance of CH₄ and especially of CO₂ are more strongly pronounced at 850 °C, suggesting routes for CH₄ and CO₂ conversion others than reforming to synthesis gas. Similarly, when working with Rh (0.5 wt%) over different type of supports [46] it was reported that the CO₂ conversion was always higher than that of CH₄ and that CO yield was always higher than H₂, and H₂/CO ratio was always below one. This result was attributed to side reactions that were taking place simultaneously with the reforming reaction.

The forward rates of CH₄ and CO₂ conversion at 650 °C increase with the increase in CO₂ concentration (Fig. 7B) up to the value corresponding to the ratio of CO₂/CH₄ = 1.5 in the feed and slows down upon the addition of excessive CO₂ due to progressive oxidation of Ni clusters. Location of rate maxima may imply competitive adsorption at the low temperature and different adsorption strengths for both reactants. At the constant CH₄ concentration, the inhibitory effect of CO₂ on the CH₄ forward rate is strongly pronounced at the temperature of 850 °C also owing to accelerated migration of reactive oxygen species being able to enhance the oxidation degree of Ni clusters and hence caused the rate of reaction to decrease. The CO₂ consumption rate increases proportional to the feed within all the range of CO₂/CH₄ ratio studied by affecting the side non-selective reactions, including direct oxidation reactions. Indeed, as it was observed [19,47], both methane and carbon dioxide dissociate and may react independently of one another on the metal site. In fact, CO₂ dissociates into carbon and two oxygen atoms on the active site and that it was possible that carbon and oxygen on the catalyst surface recombine to form CO. As CO₂ is converted into CO, and CH₄ can be converted into CO, CO₂, H₂, and H₂O, this implies that besides the reverse water gas shift reaction, several side reactions may occur in the dry reforming, including CO disproportionation reaction (3), CO/H₂ reduction reaction, CO₂/H₂

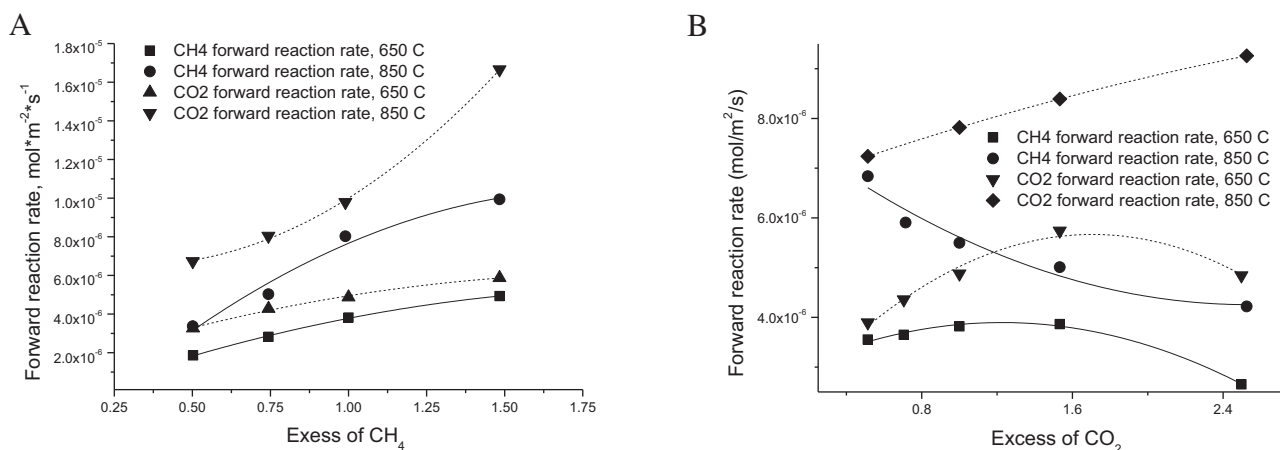


Fig. 7. The forward reforming rates of CO₂ reforming of CH₄ depending on excess of CH₄ (A) and CO₂ (B) over stoichiometric values in the feed: a catalyst – Pt+Ni/PrSmCeZrO/YSZ; a feed mixture – 7% CH₄ + 7% CO₂, balance N₂; W/F=0.0052 g s/ml (3.6 ms residence time).

methanation reaction ($\text{CO}_2 + 4\text{H}_2 = \text{CH}_4 + 2\text{H}_2\text{O}$) and CO/ H_2 methanation reaction ($\text{CO} + 3\text{H} = \text{CH}_4 + \text{H}_2\text{O}$).

4.3.3. Effect of the reaction temperature

The temperature effect was investigated at atmospheric pressure at 650, 700, 750, 800 and 850 °C and the reactant feed gas 7% CH_4 + 7% CO_2 + nitrogen balance. Fig. 8 shows the effect of the reaction temperature on CH_4 and CO_2 forward rates and product ratios for the specified residence times. The reaction rates of both CH_4 and CO_2 increase monotonically with increasing reaction temperature (Fig. 8A). As shown in Fig. 8B, increasing the temperature causes an increase in H_2/CO and decrease in CO_2/CO ratios. This means that by increasing temperature, there is more synthesis gas in the product. Increasing the residence time resulted in a further increase in selectivity to the desired product. Thus, at the highest value of the residence time –30 ms ($F = 5.64 \text{ l/h}$, $W = 68 \text{ mg}$), the maximum concentrations of syngas in the product gas were found to be 22.7% v/v with the H_2 to CO ratio of 0.975, at 750 °C (77% H_2 yield and 90% CO yield), 23.7% v/v with 0.982 at 800 °C (83.5% H_2 yield and 93.7% CO yield) and 23.7% v/v with 0.972 at 850 °C. Simultaneously, the corresponding values of CO_2/CO ratios were 0.04, 0.03, 0.02.

4.3.4. Reaction order with respect to the reactants

The amount of catalyst employed in the reforming reaction was 15.3 mg. Pellet and bed gradients were eliminated using dilution strategies. The partial pressure of N_2 was tuned to control the total flow rate of the gases at 10.62 l/h. The forward rates for CH_4 and CO_2 reforming over the Pt + Ni/PrSmCeZrO/YSZ catalyst were proportional to CH_4 concentration (Fig. 7A). The reaction order with respect to each of the feed components was calculated at 650 and 850 °C. The plots of logarithm of the CH_4 forward reaction rates against logarithm of the partial pressure of the components for the dry reforming at different temperatures are shown in Fig. 9. The reaction orders were calculated according to the line slopes. Forward CH_4 reaction rates increased linearly with increasing CH_4 partial pressure in the feed mixture. It was shown that kinetics assumption of the first-order in CH_4 is valid at almost all operating conditions up to the equimolar ratio in the feed within experimental accuracy. This is in agreement with methane dry reforming data on various noble metal catalysts reported by Iglesia and co-workers [32,48–50]. Weak inhibition was also observed by the CH_4 excess over stoichiometric value. At low temperatures, the relatively constant, zero order in CO_2 can be applied in the range of CO_2 excess 1.5 over stoichiometric value (apparent reaction order is equal 0.08). The inhibitory effect of CO_2 excess increases with increasing temperature. An excess of CO_2 acts as inhibitor or surface site blocker, that results in the formation of less H_2 (Fig. 6B), and apparent reaction order (Fig. 9B) becomes negative (–0.7) at the higher CO_2/CH_4 ratio.

A strong inhibitory effect of CO_2 excess in the case of Ni-containing catalysts in comparison with Pt supported on traditional supports (alumina, zirconia, magnesia) [51–53] catalysts might be explained by a combination of the following factors:

- Much higher ability of Ni to be oxidized by CO_2 ;
- Strong effect of stabilization of Ni cations by interaction with fluorite-like support;
- High surface oxygen mobility in fluorite-like supports providing fast supply of oxygen species produced by CO_2 dissociation on the surface oxygen vacancies to Ni clusters, which also help to increase their oxidation. This is the principal difference between fluorite-like complex oxides and traditional supports. In most cases, activation of CO_2 on support surface is either hardly possible or occurs via formation of inherently much less reactive carbonates.

- Apparent domination of Ni atoms on the surface of catalyst due to its much higher concentration. Hence, specificity of catalytic properties and kinetics is apparently determined by chemistry and structure of Ni clusters, while Pt atoms incorporated into these clusters could be mainly responsible for their disordering, thus helping to increase their ability to rupture C–H bond in CH_4 molecule and prevent nucleation of carbon species (fibers, graphitic species etc.).

Therefore, more studies are needed to elucidate inhibitory effect of CO_2 excess, particularly at elevated temperatures.

4.3.5. Activation energies with respect to reactant consumption and product formation

Activation energy is different over different catalysts. Within the wide range of activation energies reported for CO_2 reforming of CH_4 (7 to 86 kcal/mol), $14.6 \pm 1 \text{ kcal/mol}$ (~61 kJ/mol) is quite frequently observed [1]. In order to minimize effects of side reactions, activation energies with respect to reactant consumption and product formation were determined by using the experimental data obtained at the low residence time (3.6 ms), where the conversions and yield of the products were far lower than correspond to thermodynamic equilibrium (Fig. 4). The logarithm of reaction rates against the reciprocal of absolute temperature were plotted in Fig. 10. The reaction behavior exhibits two different kinetic regimes with different activation energies: a higher activation energy regime in the range of 650–750 °C and a lower activation energy regime in the range of 750–850 °C. Inflection is observed at about 750 °C in all of the plots, indicating that an increase in the reaction temperature over 750 °C leads to inhibition in the reforming reaction. In general, changes in the slope of an Arrhenius plot indicate a change in the rate-determining step of a reaction. The reaction order of CO_2 (Fig. 9B) varies with the reaction temperature also, that proves the suggestion. The calculated activation energies in the two temperature regions were found to be 43.8 and 41.1 for CH_4 and CO_2 forward reaction rate and 61.0 and 39.6 kJ/mol for H_2 and CO formation below 750 °C, and 18.2, 14.0, 29.8 and 18.8 kJ/mol, respectively, above 750 °C. The proximity of activation energy values for CH_4 , CO_2 , and CO in both low and high temperature regions suggests that the rate controlling steps for CO formation are the same as that for CH_4 and CO_2 consumption. The route of hydrogen formation seems to be more temperature sensitive in the both temperature regions. The highest activation energy value for H_2 formation might be attributed to the fact that the rate limiting step in entire sequence of elementary steps comprising the reforming reaction is in the route for formation of hydrogen.

However, we shall suppose another reason of the inflexion observed for the plots at the temperature of about 750 °C. Despite the care taken to minimize diffusion control, pore diffusion limited regime is probably taking place at temperatures above 750 °C when the activation energies are roughly one half of the corresponding values below 750 °C. Further study will need to clarify and examine these issues.

4.4. Proposition of a steady state rate equation

There is no generally accepted kinetic model available for CO_2 reforming of CH_4 . A Langmuir–Hinshelwood type of model has been most often used in the kinetic studies of CO_2 reforming of CH_4 [1,54–58]. For the Pt + Ni/PrSmCeZrO/YSZ nanocomposite catalyst, a kind of Pt–Ni interactions certainly exists, which is responsible for variations in the dissociative adsorption capacity of methane and carbon dioxide. It would be interesting to analyze the kinetic scheme (15) to deduce a kinetic equation for the rate of CH_4 transformation, when the reaction occurs under steady-state conditions. For the Pt/PrSmCeZrO oxide catalyst, the $[\text{O}_s]$ intermediates con-

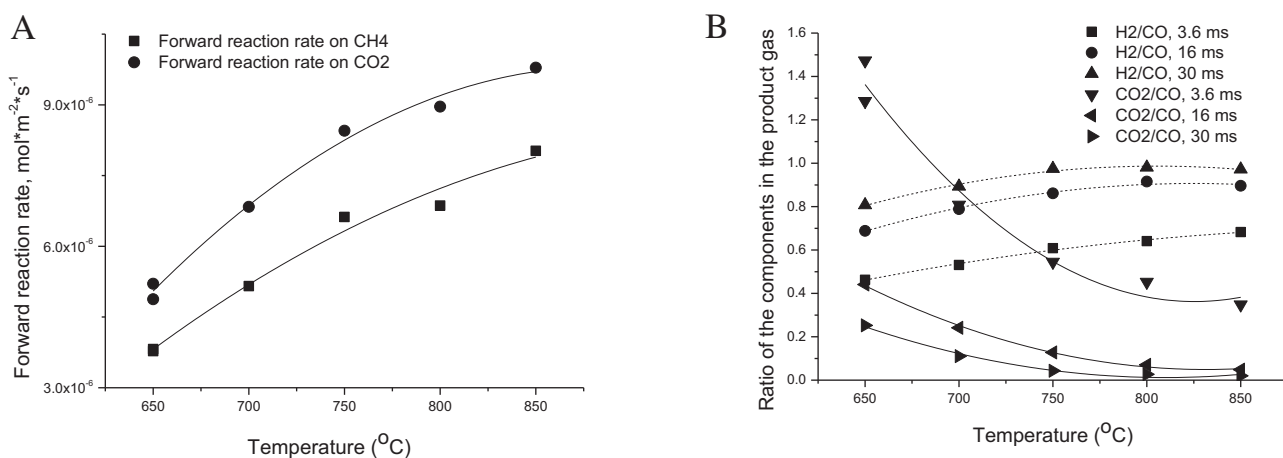


Fig. 8. Effect of the reaction temperature on the forward reaction rate (A) and the ratio of components in the product gas (B): a catalyst – Pt + Ni/PrSmCeZrO/YSZ; a feed mixture – 7% CH_4 + 7% CO_2 , balance N_2 ; $W/F = 0.0052 \text{ g s/ml}$ (3.6 ms residence time).

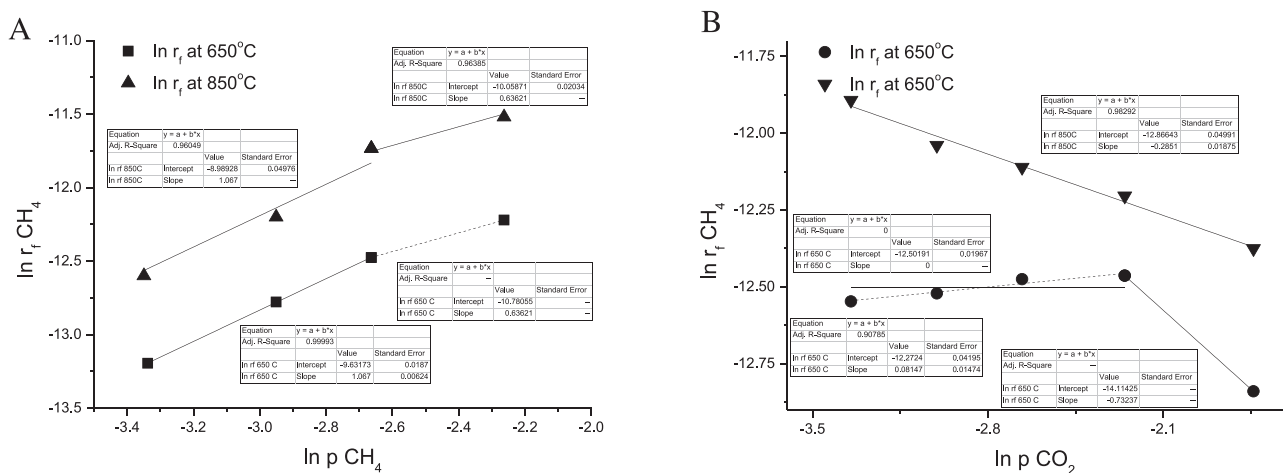


Fig. 9. The plots of $\ln r_f \text{CH}_4$ (A) against $\ln p \text{CH}_4$ and $\ln r_f \text{CH}_4$ (B) against $\ln p \text{CO}_2$: a feed mixture – 7% CH_4 + 7% CO_2 , balance N_2 ; $W/F = 0.0052 \text{ g s/ml}$ (3.6 ms residence time).

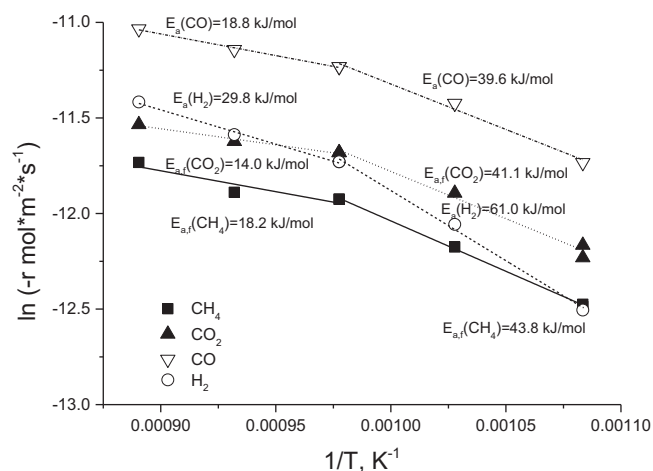


Fig. 10. Arrhenius plots for CH_4 , CO_2 , CO and H_2 : a feed mixture – 7% CH_4 + 7% CO_2 , balance N_2 ; $W/F = 0.0052 \text{ g s/ml}$ (3.6 ms residence time).

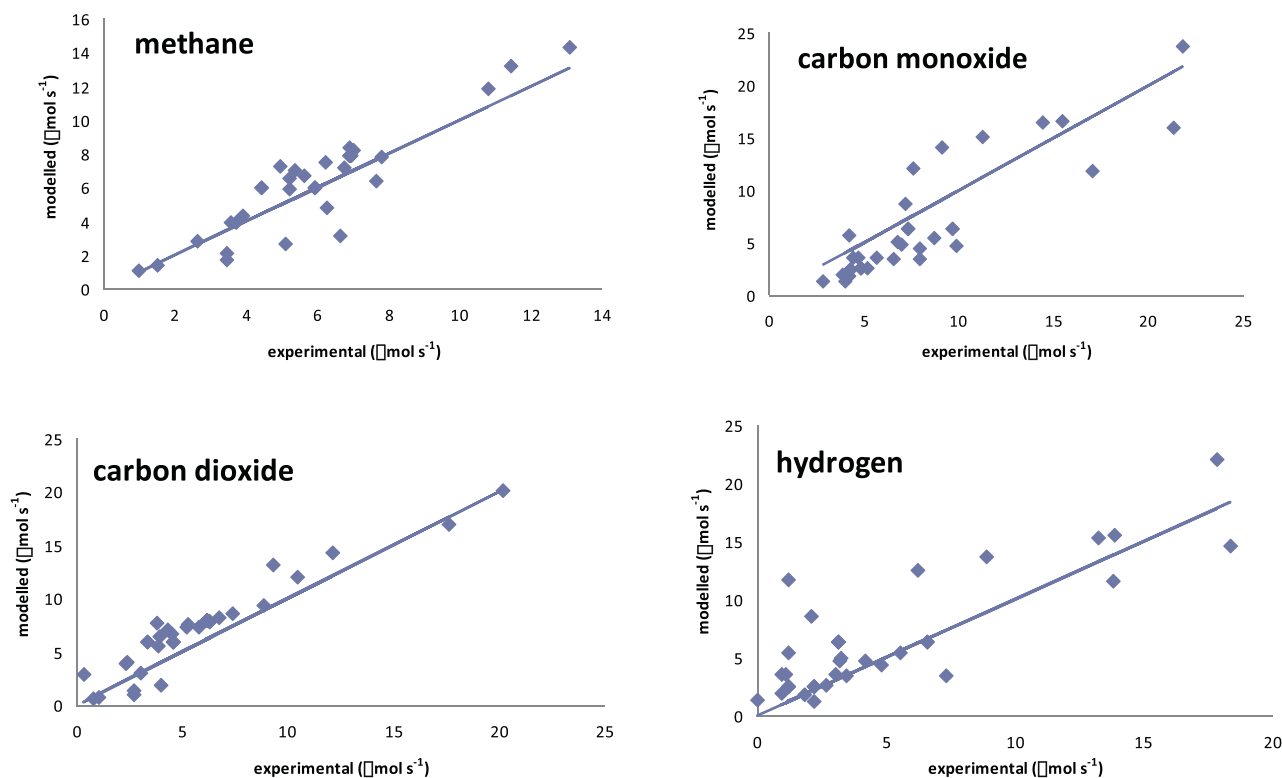


Fig. 11. Parity diagrams of CO₂ reforming of CH₄.

centration on the catalyst surface is rather high and does not vary much, whereas the surface coverage by carbonates is rather low and they are reversibly adsorbed on the surface sites [44]. These results allow to take some assumptions and to linearize the reaction network. To obtain the first approximation for the kinetic equation under steady-state conditions, the following simplifications could be used for the rates of catalytic steps also: (a) [MeCO₃] concentration on the surface (where Me is Pt or Ni) is significantly lower than the surface concentration of oxidized Me-centers [PtO or NiO], (b) the rate of step 4 in the forward direction is significantly higher than that in the reverse direction; (c) [MeO] concentration varies negligibly in the step 6, Eq. (15).

Under steady-state conditions the time derivatives of [MeO] and [MeCO₃] coverage are equal to zero and the concentration of the intermediates is determined by reagent concentrations in the gas phase. For the assumptions given above [MeO] coverage value is

defined by steps 3 and 4 and [MeCO₃] coverage value is expressed from the rates of steps 1 and 2. Preliminary simplified forms of kinetic equations for the rates of CH₄ transformation look as follows:

$$r_2 = \frac{k_1 k_2 k_4 \rho_{\text{CH}_4} \rho_{\text{CO}_2}^2}{(k_{-1} k_2 \rho_{\text{CH}_4}) (k_3 \rho_{\text{CH}_4} + k_4 \rho_{\text{CO}_2})} = \frac{k_1 k_2 k_4 \rho_{\text{CH}_4} \rho_{\text{CO}_2}}{(k_{-1} k_2 \rho_{\text{CH}_4}) (k_4 + k_3 \rho_{\text{CH}_4} / \rho_{\text{CO}_2})} \quad (16)$$

$$r_3 = \frac{k_2 k_4 \rho_{\text{CH}_4} \rho_{\text{CO}_2}}{(k_3 \rho_{\text{CH}_4} + k_4 \rho_{\text{CO}_2})}$$

4.5. Model regression to experimental data

A regression analysis of the above equations against a data set consisting of 36 measurements has revealed that the dry reforming rates are practically independent of the CO₂ partial pressure in the feed. A first order rate equation in CH₄ and zero order in CO₂ results

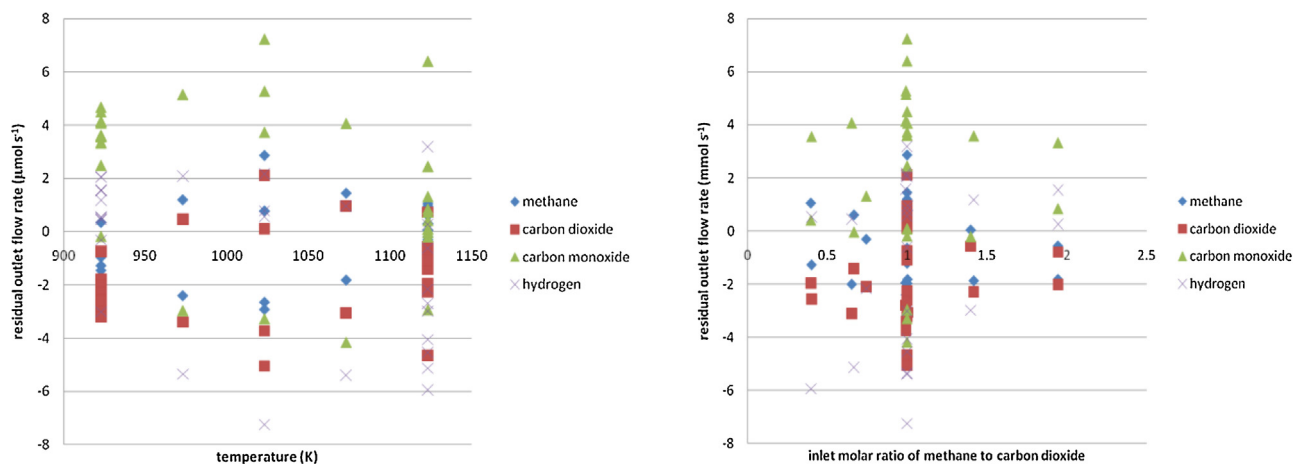


Fig. 12. Residual diagrams of the response outlet flow rates as a function of the temperature (left) and of the inlet molar ratio of methane to carbon dioxide (right).

Table 2

Kinetic parameter values obtained from model regression to experimental data at the average temperature of 677 °C.

Parameter	Estimate	Unit
k_{Tave}	2.80×10^{-2}	$\mu\text{mol}_{\text{CH}_4} \text{ s}^{-1} \text{ Pa}^{-1} \text{ kg}_{\text{cat}}^{-1}$
E	114	kJ mol^{-1}

in the best agreement between model simulations and experimental data with an F value for the global significance of the regression amounting to 112, see parity diagrams in Fig. 11.

It is an indication that most of the methane is consumed via Reaction (3) from the above reported Scheme (15), since the corresponding net reaction rate equation is reduced to a proportional relationship with the methane partial pressure on the condition that $k_4 \gg k_3$. An apparent activation energy of 114 kJ mol^{-1} is in agreement with typically reported values for dry reforming [1,22,59,60], see Table 2.

Any attempt to increase the complexity of the kinetic model and, hence, account in more detail for the actual reaction mechanism, has led to significant correlation between the adjustable model parameters and statistically insignificant parameter estimates. It means that the maximum of kinetic information has been extracted from the data by the first order rate equation in the methane partial pressure. The residual diagrams presented in Fig. 12 indeed do not indicate any significant trends for any of the responses considered.

5. Conclusion

A kinetic assessment of a Pt + Ni/PrSmCeZrO/YSZ nanocomposite catalyst in the CH_4 dry reforming was performed over a wide range of reactant ratios and reaction conditions. The nanocomposite catalyst comprised of NiO and YSZ exhibits higher conversions and selectivities than the Pt/PrSmCeZrO oxide catalyst. According to experimental data, the yield of the main products is far from equilibrium at the residence time lower than 30 ms. As long as residence times are kept long enough (≥ 30 ms), concentrations of CO , H_2 , CH_4 and CO_2 in product gas, approach those calculated assuming thermodynamic equilibrium at the reaction temperatures ≥ 750 °C.

The first-order in CH_4 reaction kinetics assumption was found to be valid for the forward reaction rate up to the equimolar reactants ratio in the feed. The reaction rate was slightly inhibited by adding CH_4 over the stoichiometric value. At low temperatures, zero order was found for CO_2 particularly when it was in a 1.5 fold excess over the stoichiometric value. The activation energies with respect to reactant consumption and product formation at the low residence time (3.6 ms) were found to be 43.8 and 41.1 for CH_4 and CO_2 forward reaction rate and 61.0 and 39.6 kJ/mol for H_2 and CO formation below 750 °C, and 18.2, 14.0, 29.8 and 18.8 kJ/mol, respectively, above 750 °C. A regression analysis performed for the net rate of CH_4 conversion over the Pt + Ni/PrSmCeZrO/YSZ catalyst confirmed that the dry reforming net rates are practically independent of the CO_2 partial pressure in the feed. A first order rate equation in CH_4 and zero order in CO_2 results in the best agreement between model simulations and experimental data.

Acknowledgement

Support by the FP7 OCMOL project as well as Russian Ministry of Education and Science is gratefully acknowledged.

References

- [1] M.C.J. Bradford, M.A. Vannice, CO_2 reforming of CH_4 , Catal. Rev.—Sci. Eng. 41 (1) (1999) 1–42.
- [2] V.V. Galvita, V.D. Belyaev, A.K. Demin, V.A. Sobyanin, Electrocatalytic conversion of methane to syngas over Ni electrode in a solid oxide electrolyte cell, Appl. Catal. A: Gen. 165 (1–2) (1997) 301–308.
- [3] T. Yamada, Y. Hiei, T. Akbay, T. Ishihara, Y. Takita, Simultaneous generation of synthesis gas and electric power by internal reforming fuel cells utilizing LaGaO_3 based electrolytes, Solid State Ionics 113–115 (11) (1998) 253–258.
- [4] H.E. Vollmar, C.U. Maier, C. Nolscher, T. Merslein, M. Poppinger, Innovative concepts for the coproduction of electricity and syngas with solid oxide fuel cells, J. Power Sources 86 (1–2) (2000) 90–97.
- [5] D. Ju Moon, W. Jo Ryu, Electrocatalytic reforming of carbon dioxide by methane in SOFC system, Catal. Today 87 (2003) 255–264.
- [6] Z. Zhan, Y. Lin, M. Pillai, I. Kim, S.A. Barnett, High-rate electrochemical partial oxidation of methane in solid oxide fuel cells, J. Power Sources 161 (1) (2006) 460–465.
- [7] M. Tucker, Progress in metal-supported solid oxide fuel cells: a review, J. Power Sources 195 (2010) 4570–4582.
- [8] I. Riess, Mixed ionic–electronic conductors—material properties and applications, Solid State Ionics 157 (2003) 1–17.
- [9] A. Atkinson, S. Barnett, R. Gorte, J. Irvine, A. Mcevoy, M. Mogensen, C.S. Singhal, J. Vohs, Advanced anodes for high-temperature fuel cells, Nature 3 (2004) 17–27.
- [10] C.M. Finnerty, N.J. Coe, R.H. Cunningham, R.M. Ormerod, Carbon formation on and deactivation of nickel-based/zirconia anodes in solid oxide fuel cells running on methane, Catal. Today 46 (1998) 137–145.
- [11] A. Dicks, Advances in catalysts for internal reforming in high temperature fuel cells, J. Power Sources 71 (1998) 111–122.
- [12] T. Takeguchi, R. Kikuchi, T. Yano, K. Eguchi, K. Murata, Effect of precious metal addition to Ni–YSZ cermet on reforming of CH_4 and electrochemical activity as SOFC anode, Catal. Today 84 (2003) 217–222.
- [13] S.M. Stagg, D.E. Resasco, et al., Effect of promoters on supported Pt catalysts for CO_2 reforming of CH_4 , in: A. Parmaliana (Ed.), Studies in Surface Science and Catalysis, vol. 119, Elsevier Science B.V., 1998, pp. 813–818, NATURAL GAS CONVERSION V.
- [14] G.S. Gallego, J.G. Marín, C. Batiot-Dupeyrat, J. Barrault, F. Mondragó, Influence of Pr and Ce in dry methane reforming catalysts produced from $\text{La}_{1-x}\text{A}_x\text{NiO}_3$, Appl. Catal. A: Gen. 369 (2009) 97–103.
- [15] V. Palma, F. Castaldo, P. Ciambelli, G. Iaquaniello, G. Capitani, On the activity of bimetallic catalysts for ethanol steam reforming, Int J. Hydrogen Energy 16 (2013) 6633–6645.
- [16] A.L. Smirnova, V.A. Sadykov, N.V. Mezentseva, R.V. Bunina, V.V. Pelipenko, G.M. Alikina, T.A. Krieger, L.N. Bobrova, O.L. Smorygo, F. van Berkel, B. Rietveld, Design and testing of structured catalysts for internal reforming of CH_4 in intermediate temperature solid oxide fuel cells (IT SOFC), ECS Trans. 35 (1) (2011) 2771–2780.
- [17] V. Sadykov, N. Mezentseva, G. Alikina, R. Bunina, V. Pelipenko, A. Lukashevich, Z. Vostrikov, V. Rogov, T. Krieger, A. Ishchenko, V. Zaikovskiy, L. Bobrova, J. Ross, O. Smorygo, A. Smirnova, B. Rietveld, F. van Berkel, Nanocomposite catalysts for steam reforming of methane and biofuels: design and performance, in: Book Nanocomposite Materials, Theory and Applications, INTECH, Austria, Vienna, 2010, pp. 909–946, ISBN 978-953-7619-X-X.
- [18] T. Kharlamova, S. Pavlova, V. Sadykov, T. Krieger, G. Alikina, C. Argiris, Catalytic properties and coking stability of new anode materials for intermediate temperature solid oxide fuel cells, Catal. Today 146 (2009) 141–147.
- [19] V. Sadykov, V. Muzykantov, A. Bobin, N. Mezentseva, G. Alikina, N. Sazonova, E. Sadovskaya, L. Gubanova, A. Lukashevich, C. Mirodatos, Oxygen mobility of Pt-promoted doped CeO_2 – ZrO_2 solid solutions: characterization and effect on catalytic performance in syngas generation by fuels oxidation/reforming, Catal. Today 157 (2010) 55–60.
- [20] V. Sadykov, V. Usoltsev, Y. Fedorova, N. Mezentseva, T. Krieger, N. Ereemeev, M. Arapova, A. Ishchenko, A. Salanovi, V. Pelipenko, V. Muzykantov, A. Ulikhin, N. Uvarov, O. Bobrenok, A. Vlasov, M. Korobeynikov, A. Bryazgin, A. Arzhannikov, P. Kalinin, O. Smorygo, M. Thumm, Advanced sintering techniques in design of planar IT SOFC and supported oxygen separation membranes, in: Book Sintering, INTECH, Austria, Vienna, 2011, ISBN 978-953-308-4-8.
- [21] J.R. Rostrup-Nielsen, J.H.B. Hansen, CO_2 -reforming of methane over transition metals, J. Catal. 144 (1993) 38–49.
- [22] M. Maestri, D.G. Vlachos, A. Beretta, G. Groppi, E. Tronconi, Steam and dry reforming of methane on Rh: microkinetic analysis and hierarchy of kinetic models, J. Catal. 259 (2008) 211–222.
- [23] V.C.H. Kroll, H.M. Swaan, C. Mirodatos, Methane reforming reaction with carbon dioxide over Ni/SiO₂ catalyst-I, Deactivation Stud. J. Catal. 161 (1) (1996) 409–422.
- [24] M. Khoshtinat Nikoo, N.A.S. Amin, Thermodynamic analysis of carbon dioxide reforming of methane in view of solid carbon formation, Fuel Process. Technol. 92 (2011) 678–691.
- [25] S. Wang, G.Q. (Max) Lu, G.J. Millar, Carbon dioxide reforming of methane to produce synthesis gas over metal-supported catalysts: state of the art, Energy Fuels 10 (1996) 896–904.
- [26] L. Topor, L. Bejan, E. Ivana, N. Georgescu, Formarea negrului de fum in reactia de conversie a metanului cu CO , Rev. Chim. Bucharest 30 (1979) 539–541.
- [27] E.P. Murray, T. Tsai, S.A. Barnett, A direct-methane fuel cell with a ceria-based anode, Nature 400 (1999) 649–651.
- [28] K. Kendall, C.M. Finnerty, G. Saunders, J.T. Chung, Effects of dilution on methane entering an SOFC anode, J. Power Sources 106 (2002) 323–327.
- [29] O. Levenspiel, Chemical Reaction Engineering, 3rd ed., Wiley, New York, 1999.

- [30] C.N. Satterfield, *Mass Transfer in Heterogeneous Catalysis*, MIT Press, 1970.
- [31] M. Boudart, G. Djega-Mariadassou, *The Kinetics of Heterogeneous Catalytic Reactions*, Princeton University Press, Princeton, NJ, 1984.
- [32] J. Wei, E. Iglesia, Structural requirements and reaction pathways in methane activation and chemical conversion catalyzed by rhodium, *J. Catal.* 225 (2004) 116–127.
- [33] M.P. Pechini, Method of preparing lead and alkaline earth titanates and niobates and coating method using the same to form a capacitor, U.S. Patent 3330697 (1967).
- [34] V. Sadykov, Y. Borchert, G. Alikina, A. Lukashevich, R. Bunina, G. Zabolotnaya, N. Mezentsseva, E. Moroz, V. Zaikovskii, D. Zyuzin, N. Uvarov, V. Zyryanov, N. Orlovskaya, One pot synthesis of mixed ionic–electronic conducting nanocomposites comprised of fluorite-like and perovskite-like phases as catalytic materials for SOFC, *Mater. Res. Soc. Symp. Proc.* 900E (2006), O10.08.
- [35] V.A. Sadykov, T.G. Kuznetsova, G.M. Alikina, Y.V. Frolova, A.I. Lukashevich, V.S. Muzykantov, V.A. Rogov, L.C. Batuev, V.V. Kriventsov, D.I. Kochubei, E.M. Moroz, D.A. Zyuzin, E.A. Paukshtis, E.B. Burgina, S.N. Trukhan, V.P. Ivanov, L.G. Pinaeva, Y.A. Ivanova, V.G. Kostrovskii, S. Neophytides, E. Kemnitz, K. Scheurell, C. Mirodatos, Ceria-based fluorite-like oxide solid solutions promoted by precious metals as catalysts of methane transformation into syngas, in: D.K. McReynolds (Ed.), *New Topics in Catalysis Research*, Nova Science Publishers, NY, USA, 2007, pp. 97–196, Chapter 5.
- [36] V. Sadykov, V. Muzykantov, A. Bobin, N. Mezentsseva, G. Alikina, N. Sazonova, E. Sadvokskaya, L. Gubanova, A. Lukashevich, C. Mirodatos, Oxygen mobility of Pt-promoted doped CeO_2 – ZrO_2 solid solutions: characterization and effect on catalytic performance in syngas generation by fuels oxidation/reforming, *Catal. Today* 157 (2010) 55–60, <http://dx.doi.org/10.1016/j.cattod.2010.03.064>.
- [37] A.L. Smirnova, V.A. Sadykov, N.V. Mezentsseva, R.V. Bunina, V.V. Pelipenko, G.M. Alikina, T.A. Krieger, L.N. Bobrova, O.L. Smorygo, F. van Berkel, B. Rietveld, Design and testing of structured catalysts for internal reforming of CH_4 in intermediate temperature solid oxide fuel cells (IT SOFC), *ECS Trans.* 35 (1) (2011) 2771–2780.
- [38] V.A. Sadykov, N.N. Sazonova, A.S. Bobin, V.S. Muzykantov, E.L. Gubanova, G.M. Alikina, A.I. Lukashevich, V.A. Rogov, E.N. Ermakova, E.M. Sadvokskaya, N.V. Mezentsseva, E.G. Zevak, S.A. Veniaminov, M. Muhler, C. Mirodatos, Y. Schuurman, A.C. van Veen, Partial oxidation of methane on Pt-supported lanthanide doped ceria–zirconia oxides: effect of the surface/lattice oxygen mobility on catalytic performance, *Catal. Today* 169 (2011) 125–137, <http://dx.doi.org/10.1016/j.cattod.2010.10.098>.
- [39] E.L. Gubanova, V.A. Sadykov, A.C. van Veen, TAP investigation on the short contact time oxidation of methane over supported Pt catalysts with oxygen storage capacity, *Prepr. Pap.—Am. Chem. Soc. Div. Pet. Chem.* 56 (1) (2011) 181–182.
- [40] A.S. Bobin, V.A. Sadykov, V.A. Rogov, N.V. Mezentsseva, G.M. Alikina, E.M. Sadvokskaya, T.S. Glazneva, N.N. Sazonova, M.Y. Smirnova, S.A. Veniaminov, C. Mirodatos, V. Galvita, G.B. Marin, Mechanism of CH_4 dry reforming on nanocrystalline doped ceria–zirconia with supported Pt, Ru, Ni, and Ni–Ru, *Topics Catal.* 56 (2013) 958–968, <http://dx.doi.org/10.1007/s11244-013-0060-z>.
- [41] V. Sadykov, V. Rogov, E. Ermakova, D. Arendarsky, N. Mezentsseva, G. Alikina, N. Sazonova, A. Bobin, S. Pavlova, Y. Schuurman, C. Mirodatos, Mechanism of CH_4 dry reforming by pulse microcalorimetry: metal nanoparticles on perovskite/fluorite supports with high oxygen mobility, *Thermochim. Acta* 567 (2013) 27–34, <http://dx.doi.org/10.1016/j.tca.2013.01.034>.
- [42] N.N. Sazonova, V.A. Sadykov, A.S. Bobin, S.A. Pokrovskaya, E.L. Gubanova, C. Mirodatos, Dry reforming of methane over fluorite-like mixed oxides promoted by Pt, *React. Kinet. Catal. Lett.* 98 (2009) 35–41.
- [43] V. Sadykov, N. Mezentsseva, V. Muzykantov, D. Efremov, E. Gubanova, N. Sazonova, A. Bobin, E. Paukshtis, A. Ishchenko, V. Voronin, J. Ross, C. Mirodatos, A. van Veen, Real structure–oxygen mobility relationship in nanocrystalline doped ceria–zirconia fluorite-like solid solutions promoted by Pt, *Mater. Res. Soc. Symp. Proc.* 1122 (2009) O05–03.
- [44] V.A. Sadykov, E.L. Gubanova, N.N. Sazonova, S.A. Pokrovskaya, N.A. Chumakova, N.V. Mezentsseva, A.S. Bobin, R.V. Gulyaev, A.V. Ishchenko, T.A. Krieger, C. Mirodatos, Dry reforming of methane over Pt/PrCeZrO catalyst: kinetic and mechanistic features by transient studies and their modelling, *Catal. Today* 171 (1) (2011) 140–149.
- [45] L. Kapokova, S. Pavlova, R. Bunina, G. Alikina, T. Krieger, A. Ishchenko, V. Rogov, V. Sadykov, Dry reforming of methane over $\text{LnFe}_{0.7}\text{Ni}_{0.3}\text{O}_{3-x}$ perovskites: influence of Ln nature, *Catal. Today* 164 (2011) 227–233, <http://dx.doi.org/10.1016/j.cattod.2010.10.086>.
- [46] H.Y. Wang, E. Ruckenstein, Carbon dioxide reforming of methane to synthesis gas over supported rhodium catalysts: the effect of support, *Appl. Catal. A: Gen.* 204 (2000) 143–152.
- [47] A.N.J. van Keulen, K. Seshan, J.H.B.J. Hoebink, J.R.H. Ross, TAP Investigations of the CO_2 Reforming of CH_4 over Pt/ZrO₂, *J. Catal.* 166 (1997) 306–314.
- [48] A. Yamaguchi, E. Iglesia, Catalytic activation and reforming of methane on supported palladium clusters, *J. Catal.* 274 (2010) 52–63.
- [49] J. Wei, E. Iglesia, Isotopic and kinetic assessment of the mechanism of reactions of CH_4 with CO_2 or H_2O to form synthesis gas and carbon on nickel catalysts, *J. Catal.* 224 (2004) 370–383.
- [50] J. Wei, E. Iglesia, Structural and mechanistic requirements for methane activation and chemical conversion on supported iridium clusters, *Angew. Chem. Int. Ed.* 43 (2004) 3685–3688.
- [51] A.I. Tsyganok, M. Inaba, T. Tsunoda, K. Suzuki, K. Takehira, T. Hayakawa, Combined partial oxidation and dry reforming of methane to synthesis gas over noble metals supported on Mg–Al mixed oxide, *Appl. Catal. A: Gen.* 275 (2004) 149–155.
- [52] Ş. Özkar-Aydinoglu, E. Özensoy, A.E. Aksoylu, The effect of impregnation strategy on methane dry reforming activity of Ce promoted Pt/ZrO₂, *Int. J. Hydrogen Energy* 34 (2009) 9711–9722.
- [53] L.V. Mattos, E. Rodino, D.E. Resasco, F.B. Passos, F.B. Noronha, Partial oxidation and CO_2 reforming of methane on Pt/Al₂O₃, Pt/ZrO₂, and Pt/Ce?ZrO₂ catalysts, *Fuel Process. Technol.* 83 (2003) 147–161.
- [54] Z. Zhang, X.E. Verykios, Mechanistic aspects of carbon dioxide reforming of methane to synthesis gas over Ni catalysts, *Catal. Today* 21 (1994) 589–595.
- [55] V.A. Tsipouriari, X.E. Verykios, Kinetic study of the catalytic reforming of methane with carbon dioxide to synthesis gas over Ni/La₂O₃ catalyst, *Catal. Today* 64 (2001) 83–90.
- [56] U. Olsbye, T. Wurzel, L. Mleczko, Kinetic and reaction engineering studies of dry reforming of methane over a Ni/La/Al₂O₃ catalyst, *Ind. Eng. Chem. Res.* 36 (1997) 5180–5188.
- [57] A. Nandini, K.K. Pant, S.C. Dhangra, Kinetic study of the catalytic carbon dioxide reforming of methane to synthesis gas over Ni–K/CeO₂–Al₂O₃, *Appl. Catal. A* 308 (2006) 119–127.
- [58] J. Zhang, H. Wang, A.K. Dalai, Kinetic studies of carbon dioxide reforming of methane over Ni–Co/Al–Mg–O bimetallic catalyst, *Ind. Eng. Chem. Res.* 48 (2009) 677–684.
- [59] M.C.J. Bradford, M.A. Vannice, Catalytic reforming of methane with carbon dioxide over nickel catalysts II. Reaction kinetics, *Appl. Catal. A: Gen.* 142 (1996) 97–122.
- [60] A.M. O'Connor, Y. Schuurman, J.R.H. Ross, C. Mirodatos, Transient studies of carbon dioxide reforming of methane over Pt/ZrO₂ and Pt/Al₂O₃, *Catal. Today* 115 (2006) 191–198.